Journal of Inorganic and Organometallic Polymers and Materials (2018) 28:585–593
https://doi.org/10.1007/s10904-017-0678-6

Modification of $Cu/Zn/Al_2O_3$ Catalyst by Activated Carbon Based Metal Organic Frameworks as Precursor for Hydrogen Production

Ali Dehghani[1] · Maryam Ranjbar[1] · Ali Eliassi[1]

Received: 18 May 2017 / Accepted: 12 September 2017 / Published online: 10 January 2018

Abstract
In this study, $Cu/Zn/Al_2O_3$-AC (AC = activated carbon) catalyst was synthesized and evaluated for dimethoxymethane (DMM) reformation to hydrogen. The $Cu/Zn/Al_2O_3$-AC catalyst was prepared using high surface area metal organic frameworks (MOFs) consisting of $Cu_3(BTC)_2$ (MOF-199) and $Zn_4O(BDC)_3$ (MOF-5) for Cu(II) and Zn(II) sources respectively, as precursors while γ-Al_2O_3 was applied as support. The synthesized catalyst was investigated by scanning electron microscopy (SEM), Fourier transform infrared spectroscopy (FT-IR), X-ray diffraction (XRD), Brunauer–Emmett–Teller analysis (BET), Temperature programmed desorption (NH_3-TPD) and Energy-dispersive X-ray spectroscopy (EDX) techniques. Complete DMM conversion was observed over $Cu/Zn/Al_2O_3$-AC catalyst (Cu:Zn:Al mole ratio of 6:3:2) under atmospheric pressure, T = 533 K, GHSV = 20 NL h^{-1} $g_{cat}{}^{-1}$, N_2/H_2O/DMM = 24/5/1 volume percent (vol%) with hydrogen productivity of 12.8 L H_2 h^{-1} $g_{cat}{}^{-1}$ and 64% hydrogen concentration. Application of MOFs as precursors and modified activated carbon as an acidic component provided the catalyst with the porous structure and high specific surface area for the hydrolysis of DMM, subsequently, high selectivity and productivity of hydrogen was obtained.

Keywords Hydrogen production · $Cu/Zn/Al_2O_3$ catalyst · Dimethoxymethane · Metal organic frameworks

1 Introduction

Fuel cells suggest great power and low weight density and are being considered for automotive and stationary power tenders [1–3]. A fuel cell is talented for portable applications with the advantages of cleanness; smallness and are considered as other environmental sources of electricity [3–5] which fuelled by H_2.

Hydrogen is great excellence secondary energy carrier, not a primary fuel, and thus has to be made from primary energy sources such as electric power or thermal [5]. Hydrogen can be produced from a variety of extensively available feed stocks, including various fossils and renewable energy sources [4–6]. Today almost 50% of hydrogen is produced by steam reforming, which for huge scale hydrogen production is the most economical way [7]. The organic compounds reforming are the main H_2 fuel source for application in fuel cell [6–8]. Earlier, the methanol fuel disadvantage is high toxicity while dimethoxymethane (DMM) is danger less chemical. Nowadays, special attention is focused on the catalytic DMM steam reforming process expansion for the H_2 generation. It has been shown that these compounds, in contrast to hydrocarbons, can be steam reformed effortlessly and selectively to hydrogen-rich gas at relatively low temperatures [9–11]. At standard conditions, DMM is liquid, so it can be easily kept and transported. It is worth emphasizing that DMM is a nontoxic, noncorrosive material with a wide possibility of usage [11–13] and is used as a unique authoritative solvent for aerosols, pump sprays in pharmaceutical and perfume industries [13–16].

The steam reforming of DMM is generally composed of the following steps [14]:

$$CH_3OCH_2OCH_3 + H_2O \rightarrow 2CH_3OH + CH_2O \quad (1)$$

$$CH_3OH + H_2O \rightarrow 3H_2 + CO_2 \quad (2)$$

$$CH_2O + H_2O \rightarrow 2H_2 + CO_2 \quad (3)$$

The general reaction can be stated as:

$$CH_3OCH_2OCH_3 + 4H_2O \rightarrow 8H_2 + 3CO_2 \quad (4)$$

✉ Maryam Ranjbar
marandjbar@gmail.com

[1] Department of Chemical Technologies, Iranian Research Organization for Science and Technology (IROST), P.O. Box 33535-111, Tehran, Iran

Efficient CuO–CeO_2/γ-Al_2O_3 catalysts have been recommended for DMM steam reforming. These catalysts cover both the surface acid sites of γ-Al_2O_3 for DMM hydration and Cu-based type for methanol/formaldehyde steam reforming [15]. Nowadays, the Cu/Zn/Al_2O_3-40% H-CNF (H-CNF = acidic carbon nanofibers) as complex catalyst displayed active performance for the reforming of DMM. Since DMM hydrolysis generated ~33% formaldehyde which is reformed more quickly than methanol, therefore, the rate of H_2 making from the DMM reforming over a suitable composite catalyst might be ~33% better than that from the reforming of methanol over Cu/Zn/Al_2O_3 [14].

MOFs are structures made up of inorganic nodes, which can either be single ions or clusters of ions, and organic linkers [17–19]. They contain potential voids which can be used for gas storage and separation, catalysis or drug delivery [19–21]. A logical and apparently simple technique to avoid combinatorial searching for innovative materials is to link together molecular building blocks displaying the wanted property. To create a robust porous material one could envisage constructing the equivalent of a ''molecular scaffold'' by connecting rigid rod-like organic moieties with unbending inorganic clusters that act as joints [21–24]. The plans used in the design of MOFs show crucial role in point of view of the wanted request. The foremost MOFs application is their catalytic activity. On the other hands, MOFs have been exploited as precursors for metal oxides nano structure fabrication [25–27]. Finding the anticipated morphologies will become conceivable by choosing appropriate MOFs precursors with special morphologies under appropriate operational conditions [18–22]. As a result, MOF-199 and MOF-5 (due to the high specific surface area and simple preparation) as Cu(II) and Zn(II) precursors were synthesized while γ-Al_2O_3 (as catalyst support) was applied to synthesize Cu/Zn/Al_2O_3-AC catalyst. The current work reports the outcomes of studies on DMM steam reforming to H_2-rich gas over the most efficient Cu/Zn/Al_2O_3-AC catalyst.

2 Experimental

2.1 Materials and Apparatus

All chemicals used in this project were of analytical reagent grade and purchased from Merck Company without any purification. X-ray diffraction patterns were gained using a Philips-PW 17C diffractometer with Cu Kα radiation (Philips PW, The Netherlands). The surface analysis of Cu/Zn/Al_2O_3-AC was carried out using a Tescan Mira II FE-SEM. Brunauer–Emmett–Teller (BET) surface area measurements and pore volumes were performed by Belsorp mini II Bel (Japan). For all X-ray diffraction (XRD) patterns reported in this study, XRD was performed under atmospheric conditions with a Philips X-Pert. FTIR spectra were documented by a Bruker IFS-66 FT-IR Spectrophotometer (Karlsruhe, Germany). The elemental analysis of samples was achieved by Energy-dispersive X-ray spectroscopy (EDX) (30XL, Philips Company, Holland). Procedure for evaluation of the catalyst was achieved with a fixed bed reactor in a catalyst testing system which was employed in earlier work [28].

2.2 Synthesis of MOF-5

Ultrasonic irradiation technique established in the literature was employed for MOF-5 fabrication [29]. At first, 1.21 g $Zn(NO_3)_2{\cdot}6H_2O$ and 0.34 g H_2BDC (Terephthalic acid) were dissolved in 40 mL DMF accomplished by ultrasonic irradiation for 1 h with a high-density ultrasonic probe. Afterward, triethylamine (1.60 g) was added drop wise to the solution. Under ultrasonic irradiation for 1 h, a colorless precipitate was gained that was gathered by centrifugation at 13,000 rpm for 10 min. At last, the resultant product cleaned by DMF for numerous times and at 373 K for 12 h was dried.

2.3 Functionalization of Activated Carbon

In the parallel step, 1.0 g of activated carbon was mixed with 100 mL of 6 M HNO_3 into a round-bottom flask and refluxed for 3 h in order to enhance carboxylic acid contents on the activated carbon surface [30]. The oxidized material was consequently washed with distilled water until neutral pH, and subsequently dried for 24 h at 383 K.

2.4 Synthesis of Modified MOF-199 with Activated Carbon

MOF-199 modification with activated carbon (MOF-199/AC) was achieved under reflux condition by the reaction of 0.84 g of H_3BTC (benzene-1,3,5-tricarboxylic acid) and 1.75 g of $Cu(NO_3)_2{\cdot}3H_2O$ in 50 mL of ethanol including 0.05 g AC similar described procedure for encapsulation of MOF-199 with Fe_3O_4 (magnetic MOF) [31]. The mixture was cooled to room temperature after 48 h and the blue powder was recovered by filtration, washed with water and ethanol and dried under vacuum at 373 K for 12 h.

2.5 Cu/Zn/Al_2O_3 Catalyst Synthesis

By incipient wetness impregnation method, Cu/Zn/Al_2O_3 catalyst with Cu:Zn:Al mole ratio of 6:3:2 was fabricated [32]. An aqueous solution containing copper(II) and zinc(II) nitrates were added drop wise onto γ-Al_2O_3 powder under vigorous stirring for 2 h. For drying, the mixture was evaporated at 373 K and then the achieved powder was calcined for 4 h at 673 K with 72% product yield.

2.6 Cu/Zn/Al_2O_3-AC Synthesis with MOF Precursor

As a new strategy, for the synthesis of Cu/Zn/Al_2O_3-AC catalyst (with Cu:Zn:Al molar ratio of 6:3:2), the MOF-199/AC and MOF-5 aqueous solution was stirred vigorously for 2 h in order to attain a homogeneous light blue mixture. Then, this mixture was added drop wise onto γ-Al_2O_3 powder to obtain a homogeneous mixture. The mixture stirred for 3 h and dried in an oven at 373 K. The resultant precipitate was calcined at 673 K for 4 h. The catalyst color was dark-brown with 54% product yield.

3 Results and Discussion

3.1 Catalysts Characterization by FT-IR, SEM-EDX, XRD, BET and NH_3-TPD Techniques

The MOF-5 FT-IR spectrum was recorded (Fig. 1). Samples are the collection of a KBr pellet spectrum of an aliquot of the powdered sample. The 1505 and 1580 cm^{-1} bands owing to the asymmetric stretching vibration of –COO while the 1335 and 1410 cm^{-1} bands are agreed with the symmetric –COO stretching vibration group. Then, the bands at 1150, 1120 and 1020 cm^{-1} represent the in-plane bending vibration of C–H and the bands at 670, 740 and 830 cm^{-1} ascribed the out-of-plane bending vibration of C–H group. These bands proved the MOF-5 synthesis (Fig. 1a) [29].

The MOF-199 FT-IR spectra (Fig. 1b) presented a 3050 cm^{-1} band related to C–H stretching vibration of aromatic groups while the bands at 1540 and 1430 cm^{-1} due to asymmetric and symmetric starching vibrations of the O–C–O group [31]. Afterward, the broad bands at 1620 and 3100–3500 cm^{-1} owing to the attendance of carboxylate groups on activated carbon surface [30].

Finally, for Cu/Zn/Al_2O_3 and Cu/Zn/Al_2O_3-AC catalysts, the strong and broad absorption bands in the 450–950 cm^{-1} region correspond to the inorganic network (Cu–O, Zn–O, and Al–O) [33]. The absorption bands at 1430, 1550 cm^{-1} corresponding to C=C, 2950 cm^{-1} to C–H aromatic, 1620 cm^{-1} to C=O attached to metallic ions and 3100–3500 cm^{-1} to O–H, while as whole, broad band implied the presence of activated carbon with carboxylate groups in the framework of Cu/Zn/Al_2O_3-AC catalyst (Fig. 1c) [30].

The surface characterization results of Cu/Zn/Al_2O_3 and Cu/Zn/Al_2O_3-AC morphology were achieved by SEM technique. As shown in Fig. 2, The Cu/Zn/Al_2O_3 catalyst micrograph displayed a non-uniform disordered structure, while Cu/Zn/Al_2O_3-AC has spherical nanoparticle morphology. The size distribution histogram of the Cu/Zn/Al_2O_3 and Cu/Zn/Al_2O_3-AC shows a comparatively uniform distribution with an average size of 120–130 and 50–60 nm respectively

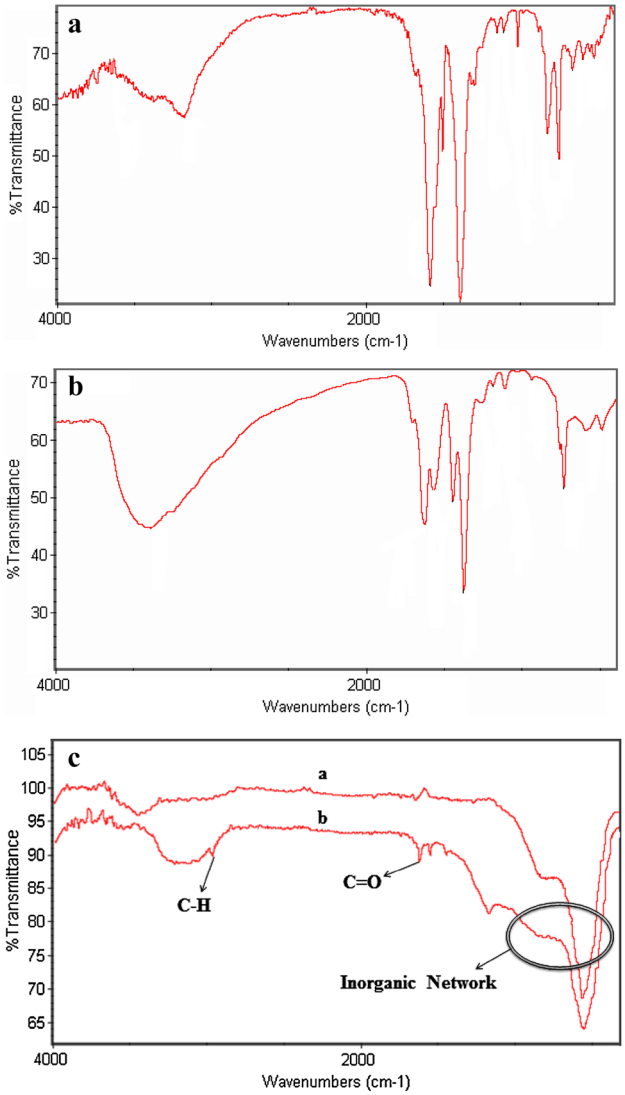

Fig. 1 FT-IR spectrum of **a** MOF-5, **b** MOF-199, **c** Cu/Zn/Al_2O_3 (*a*) and Cu/Zn/Al_2O_3-AC (*b*)

and proved by using metal organic frameworks as a precursor, the catalyst particle size is reduced compared to the catalyst that was organized by metal salts.

For better catalysts investigation, EDX analysis was exploited (Fig. 3). The EDX spectrum of Cu/Zn/Al_2O_3 catalyst demonstrates the presence of Al, Cu, Zn, and O while for Cu/Zn/Al_2O_3-AC catalyst, the elements of Al, Cu, Zn, O, and C was displayed (Table 1). This analysis indicates the purity of the product.

XRD as a rapid analytical technique principally was done for phase identification of a catalyst crystalline material and can afford information. Figure 4 displays the XRD of MOFs powder pattern. The MOF-5 XRD pattern (Fig. 4a) illustrated high crystallinity with sharp reflection peaks in the range of 10–50°. The main characteristic peaks at $2\theta = 13.8$, 15.4, 17.9, 19.5, 20.5, 22.5, 24.7,

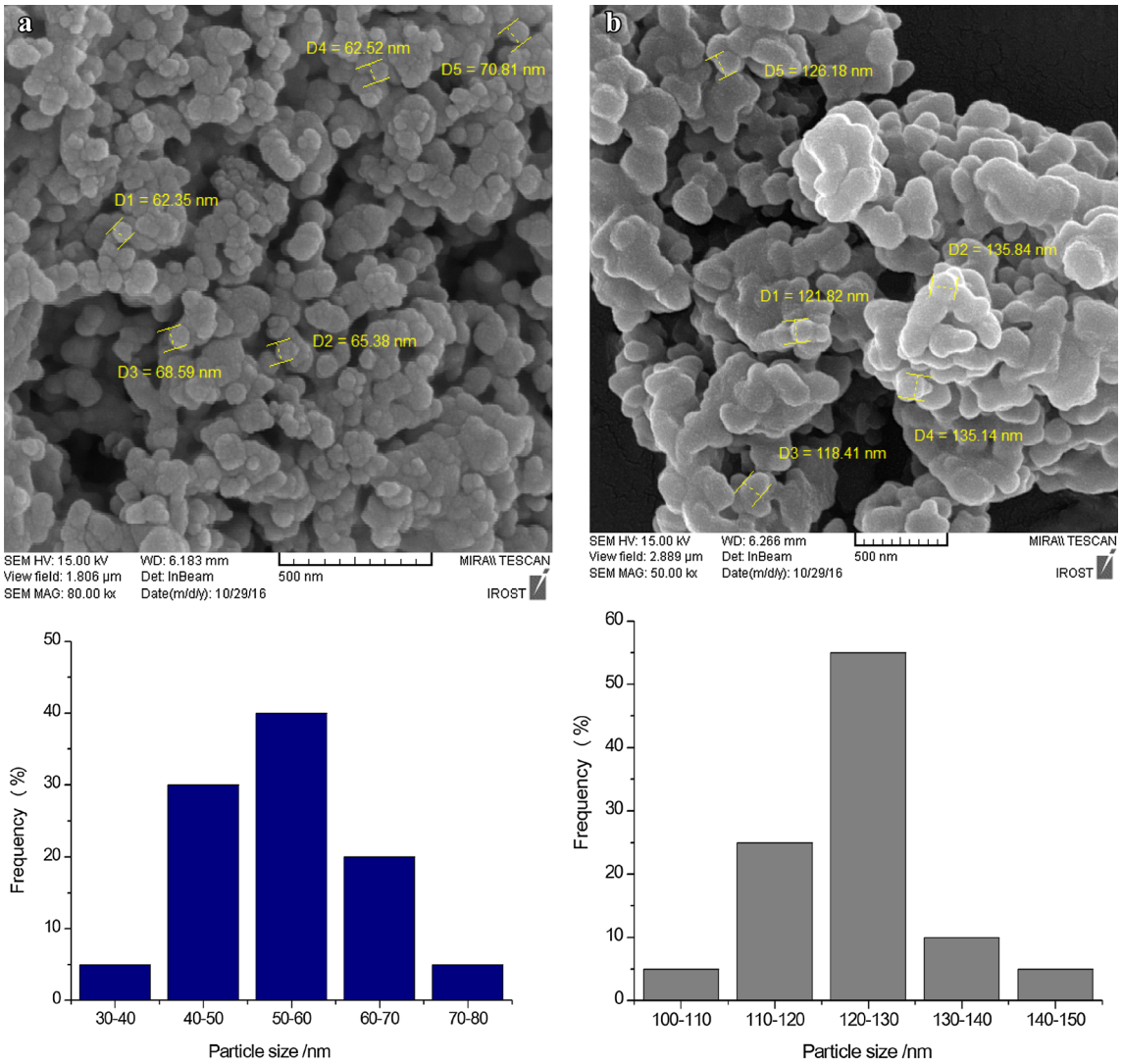

Fig. 2 SEM images of **a** $Cu/Zn/Al_2O_3$-AC, **b** $Cu/Zn/Al_2O_3$ and the size distribution histogram of the prepared catalysts

26.6, 29.8, 31.5, 34.7, 36.1 and 38.2 were the same as MOF-5 standard data and proves fruitful MOF-5 synthesis [29]. Figure 4b demonstrates the MOF-199/AC diffraction peaks in the range of 10–50°. All of the diffraction peaks displayed that the MOF sketch crystal is fine retained even after the modification with activated carbon which agrees with the previous report [34]. Finally, the XRD pattern of $Cu/Zn/Al_2O_3$-AC and $Cu/Zn/Al_2O_3$ in the range of 30–80° showed special peaks that related to CuO and ZnO phases as presented in Fig. 5. All samples conserved their gross crystallinity after the incorporation of Cu(II) and Zn(II) (metal salts or MOF) onto the support matrix (γ-Al_2O_3). The crystalline phases of copper oxide and zinc oxide of the freshly organized catalysts were tenorite (CuO) and zincite (ZnO). Alumina and activated carbon are amorphous, so did not display any special peak in the patterns, but the intensity of the peaks reduced [14, 32].

The BET analysis is usually employed for determining surface areas of catalysts. The isotherms of nitrogen adsorption–desorption accomplished by BJH pore size distributions for the $Cu/Zn/Al_2O_3$ and $Cu/Zn/Al_2O_3$-AC catalysts were shown in Fig. 6. Based on BET analysis, the surface area of the obtained $Cu/Zn/Al_2O_3$ catalyst was 20 m^2g^{-1} with the total pore volume of 0.126 cm^3g^{-1} which were meaningfully lower than $Cu/Zn/Al_2O_3$-AC with 303 m^2g^{-1} surface area and total pore volume of 0.537 cm^3g. The $Cu/Zn/Al_2O_3$ isotherm related to nonporous and non-wetting solids (type III) with the weak interaction between adsorbent and desorbent based on IUPAC cataloging. The $Cu/Zn/Al_2O_3$-AC isotherm agreed with type IV with an H_3 hysteresis loop, mesoporous morphologies characteristic with slit-shaped and non-rigid pores. The gained data established the more porous morphology and available active sites for $Cu/Zn/Al_2O_3$-AC compared to $Cu/Zn/Al_2O_3$ [35, 36].

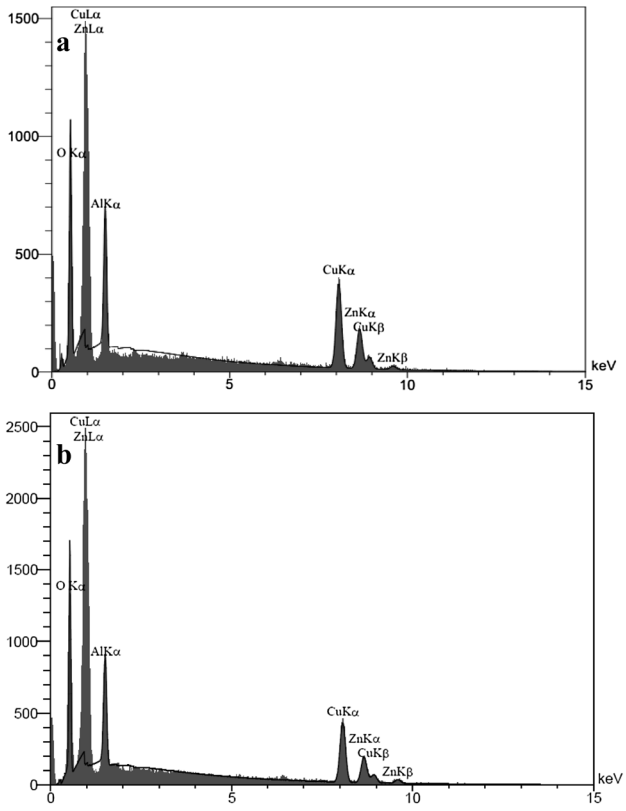

Fig. 3 EDAX spectrum of **a** $Cu/Zn/Al_2O_3$-AC and **b** $Cu/Zn/Al_2O_3$

NH_3–TPD technique affords information on the strength and amount of acid sites by using NH_3 as a basic probe molecule. The peaks in the NH_3–TPD profiles are classified to three acid sites types with different acid strengths. As shown in Fig. 7, two catalysts show three desorption peaks located at 100–200, 300–500 and 600–800 °C, corresponding to weak, medium and strong surface acidity respectively [37] and $Cu/Zn/Al_2O_3$-AC catalyst has the higher amount of acidic sites as compared to $Cu/Zn/Al_2O_3$ catalyst (amount of desorbed NH_3 ($mmol/g_{cat}$) for $Cu/Zn/Al_2O_3$ and $Cu/Zn/Al_2O_3$-AC were 2.53 and 5.86 respectively).

3.2 Catalytic Performance Tests

The catalytic reactions for the hydrolysis and reforming of DMM were done in a fixed-bed reactor. For investigation of the performance of the synthesized catalyst, at each experiment, 1.0 g of the catalyst was loaded into the reactor with stainless steel grid at both ends. The catalysts were pre-reduced in situ at 553 K for 2 h using 5 vol% H_2 in N_2 and then the temperature was diminished to 473 K. The catalysts were exposed to the feed composed of N_2/H_2O/DMM with 24/5/1 ratio (vol%). The gas hourly space velocity (GHSV) was tuned to 20 NL h^{-1} g_{cat}^{-1}. The tests were completed at atmospheric pressure and 493, 513, 533, 553, 573 K temperature while the products were sent to GC analyzer (Teif-Gostar Co, Iran).

The steam reforming of DMM is generally composed of the following steps [14]:

$$CH_3OCH_2OCH_3 + H_2O \rightarrow 2CH_3OH + CH_2O \quad (5)$$

$$CH_3OH + H_2O \rightarrow 3H_2 + CO_2 \quad \Delta H^{\circ}_{298} = +49.4\ \text{kJ/mol} \quad (6)$$

$$CH_2O + H_2O \rightarrow 2H_2 + CO_2 \quad (7)$$

The general reaction can be stated as:

$$CH_3OCH_2OCH_3 + 4H_2O \rightarrow 8H_2 + 3CO_2 \quad (8)$$

The methanol steam reforming (MSR) (reaction 2) can be including as a combination of methanol decomposition and water–gas shift reactions:

$$CH_3OH \leftrightarrow CO + 2H_2 \quad \Delta H^{\circ}_{298} = +92\ \text{kJ/mol} \quad (9)$$

Table 1 EDX analysis of $Cu/Zn/Al_2O_3$ and $Cu/Zn/Al_2O_3$-AC catalysts

Quantitative results for $Cu/Zn/Al_2O_3$							
Elt	Line	Int	K	Kr	W%	A%	ZAF
O	Ka	307.6	0.3192	0.1989	44.40	71.21	0.4480
Al	Ka	245.9	0.0718	0.0447	11.88	11.30	0.3765
Cu	Ka	260.1	0.3935	0.2452	28.15	11.37	0.8710
Zn	Ka	117.7	0.2155	0.1343	15.57	6.11	0.8628
Quantitative results for $Cu/Zn/Al_2O_3$-AC							
Elt	Line	Int	K	Kr	W%	A%	ZAF
C	Ka	9.2	0.0253	0.0139	8.46	16.38	0.1647
O	Ka	245.1	0.2839	0.1562	41.86	60.88	0.3732
Al	Ka	204.3	0.0666	0.0366	9.47	8.16	0.3870
Cu	Ka	232.6	0.3928	0.2161	25.21	9.23	0.8573
Zn	Ka	113.2	0.2314	0.1273	15.01	5.34	0.8484

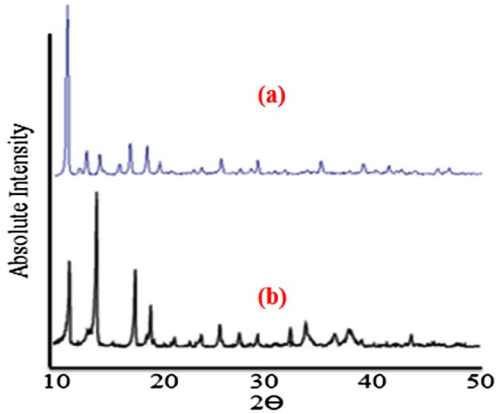

Fig. 4 XRD patterns of (*a*) MOF-199 and (*b*) MOF-5

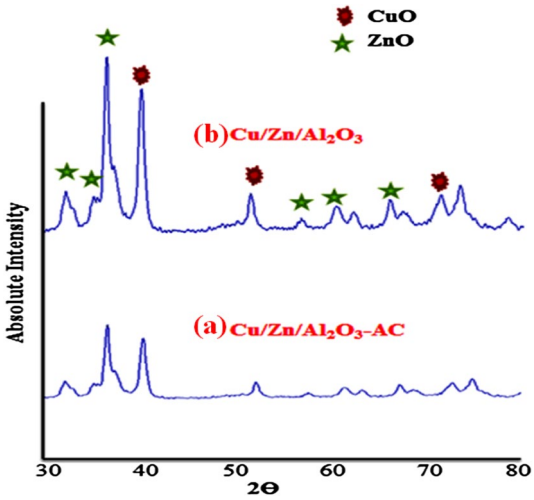

Fig. 5 XRD patterns of (*a*) $Cu/Zn/Al_2O_3$-AC and (*b*) $Cu/Zn/Al_2O_3$

$$CO + H_2O \leftrightarrow CO_2 + H_2 \quad \Delta H^{\circ}_{298} = -41.1 \text{ kJ/mol} \tag{10}$$

Methanol decomposition reaction is a reversion of methanol production reaction from synthesis gas (H_2 and CO). According to the enthalpy of reaction, this is an endothermic reaction, therefore MSR reaction goes toward the production of carbon monoxide as temperature goes up (reaction 9) and cause the production of carbon monoxide as a by-product [38]. Hence CO as the main byproduct was studied while the other byproducts were discarded.

Equations (11)–(14) were employed for DMM conversion, H_2 selectivity, H_2 yield and H_2 productivity (W_{H2}) calculations:

$$\text{DMM conversion } (\%) = \frac{mol\ (\text{DMM}_{in} - \text{DMM}_{out})}{mol\ (\text{DMM}_{in})} \times 100 \tag{11}$$

$$H_2 \text{ selectivity } (\%) = \frac{mol\left(H_{2_{out}}\right)}{mol\ (H_{2_{out}} + CO_{out})} \times 100 \tag{12}$$

$$\text{Yield}(\%) = \left(\text{DMM conversion} \times H_2 \text{ selectivity}\right) \times 100 \tag{13}$$

$$W_{H_2}\left(L\ g_{cat}^{-1} h^{-1}\right) = \frac{F \times C_{H_2}}{100 \times m_{cat}} \tag{14}$$

where C_{H_2} is the outlet hydrogen concentration and F is the total flow rate of the inlet reaction mixture ($L\ h^{-1}$) [39].

The reaction temperature effect on the DMM conversion over $Cu/Zn/Al_2O_3$ and $Cu/Zn/Al_2O_3$-AC catalysts was investigated. The H_2 is the main product of DMM conversion was monitored. The temperature has an important influence on the products distribution. As shown in Fig. 8a, the DMM conversion progressively increased for both catalysts with increasing temperature from 493 up to 573 K. $Cu/Zn/Al_2O_3$ displayed lower DMM conversion (82%), however, $Cu/Zn/Al_2O_3$-AC offered a 100% conversion due to more porous structure and acidic sites.

H_2 and CO selectivity evolution were regularly decreased and increased respectively with the reaction temperature increasing (Fig. 8b, c). The highest H_2 selectivity was detected over $Cu/Zn/Al_2O_3$-AC (97.3% at 493 K). Likewise, a high H_2 selectivity of 93.2% at 493 K was detected with $Cu/Zn/Al_2O_3$. On the other hand, the highest CO selectivity was obtained with $Cu/Zn/Al_2O_3$ (9.4% at 573 K) and $Cu/Zn/Al_2O_3$-AC catalyst showed lower CO selectivity (5.1% at 573 K).

In addition, H_2 yield as a catalytic performance indicator was assessed so that the H_2 yield enhances with the reaction temperature increases up to 533 K and then the yield of reaction remained constant with temperature increasing (Fig. 8d).

Figure 8e shows the reaction temperature effect on the H_2 concentration over $Cu/Zn/Al_2O_3$ and $Cu/Zn/Al_2O_3$-AC catalysts. As can be seen, H_2 concentration increases with the reaction temperature increase up to 533 K and reach to 64% and 53% for $Cu/Zn/Al_2O_3$-AC and $Cu/Zn/Al_2O_3$ catalysts respectively and then the concentration of H_2 remained constant approximately with temperature increasing up to 573 K.

As a result, 533 K was the best temperature for the H_2 generation with high conversion of DMM and lower production of CO in compared with the higher temperatures. High DMM conversion and also, high selectivity and yield of $Cu/Zn/Al_2O_3$-AC respect to H_2 production, can be related to its higher specific surface area and accessible acidic active sites in comparison with $Cu/Zn/Al_2O_3$.

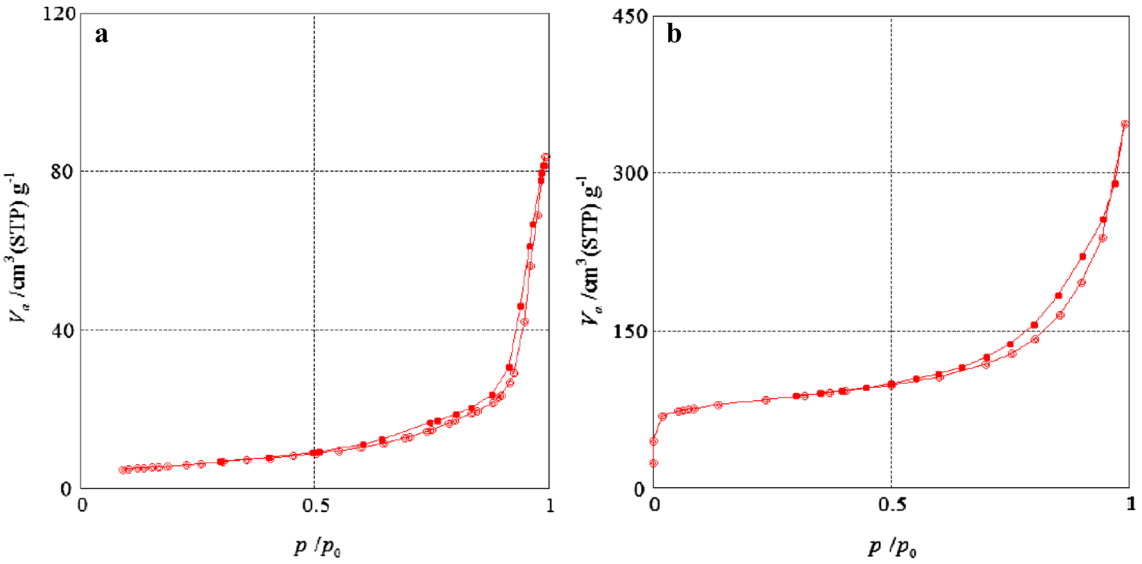

Fig. 6 Nitrogen adsorption–desorption isotherms for the **a** $Cu/Zn/Al_2O_3$-AC and **b** $Cu/Zn/Al_2O_3$

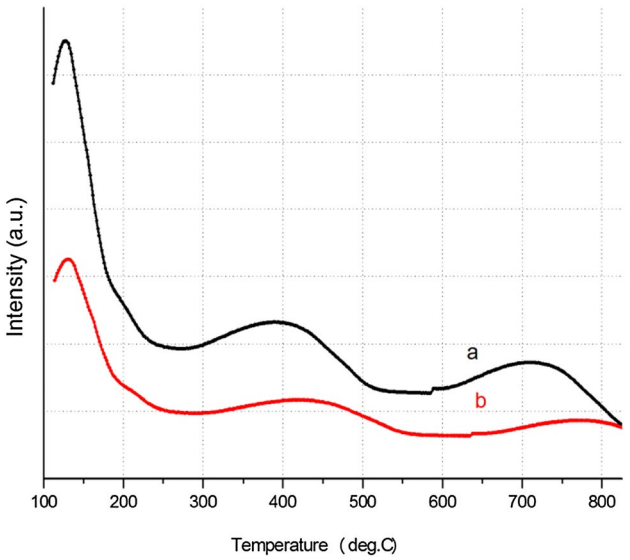

Fig. 7 NH_3–TPD profiles of (*a*) $Cu/Zn/Al_2O_3$-AC and (*b*) $Cu/Zn/Al_2O_3$

These results showed that the activity of $Cu/Zn/Al_2O_3$-AC catalyst was meaningfully better than $Cu/Zn/Al_2O_3$.

3.3 Effects of GHSV and H_2O to DMM Ratio

The effects of GHSV changes on DMM conversion was investigated in the domain of 25–35 NL h^{-1} $g_{cat}{}^{-1}$ at 533 K. Fig. 9a shows that DMM conversion was decreased by increasing GHSV for both catalysts. So that, for $Cu/Zn/Al_2O_3$-AC and $Cu/Zn/Al_2O_3$ catalysts with GHSV increasing, the conversion of DMM was decreased from 96% to 91% and 77% to 74% respectively.

The effect of H_2O/DMM ratios (1–5, v/v) on the conversion of DMM by $Cu/Zn/Al_2O_3$ and $Cu/Zn/Al_2O_3$-AC catalysts are shown in Fig. 9b (T = 533 K). The DMM conversion slowly enhanced by H_2O/DMM increasing up to 4 ratios, afterward, the DMM conversion remained constant up to 5 ratios. As can be seen, the same results were obtained for both catalysts.

4 Conclusion

As a novel approach, DMM can be successfully reformed to hydrogen on specially planned $Cu/Zn/Al_2O_3$-AC multipart catalysts. In addition, MOF as porous precursor nanomaterial provides catalysts with the larger surface area available for DMM conversion for the DMM to access the substrate, which may improve the performance of the catalyst. In this work, exploited MOFs, (MOF-199 and MOF-5) as precursors, were afforded extensive surface area in order to prepare porous catalysts for gas phase selective conversion of DMM to H_2 and subsequently higher selectivity and productivity of H_2. The addition of an acidic component with proper nature and strength can be a good proposal for the DMM reforming. Step by step

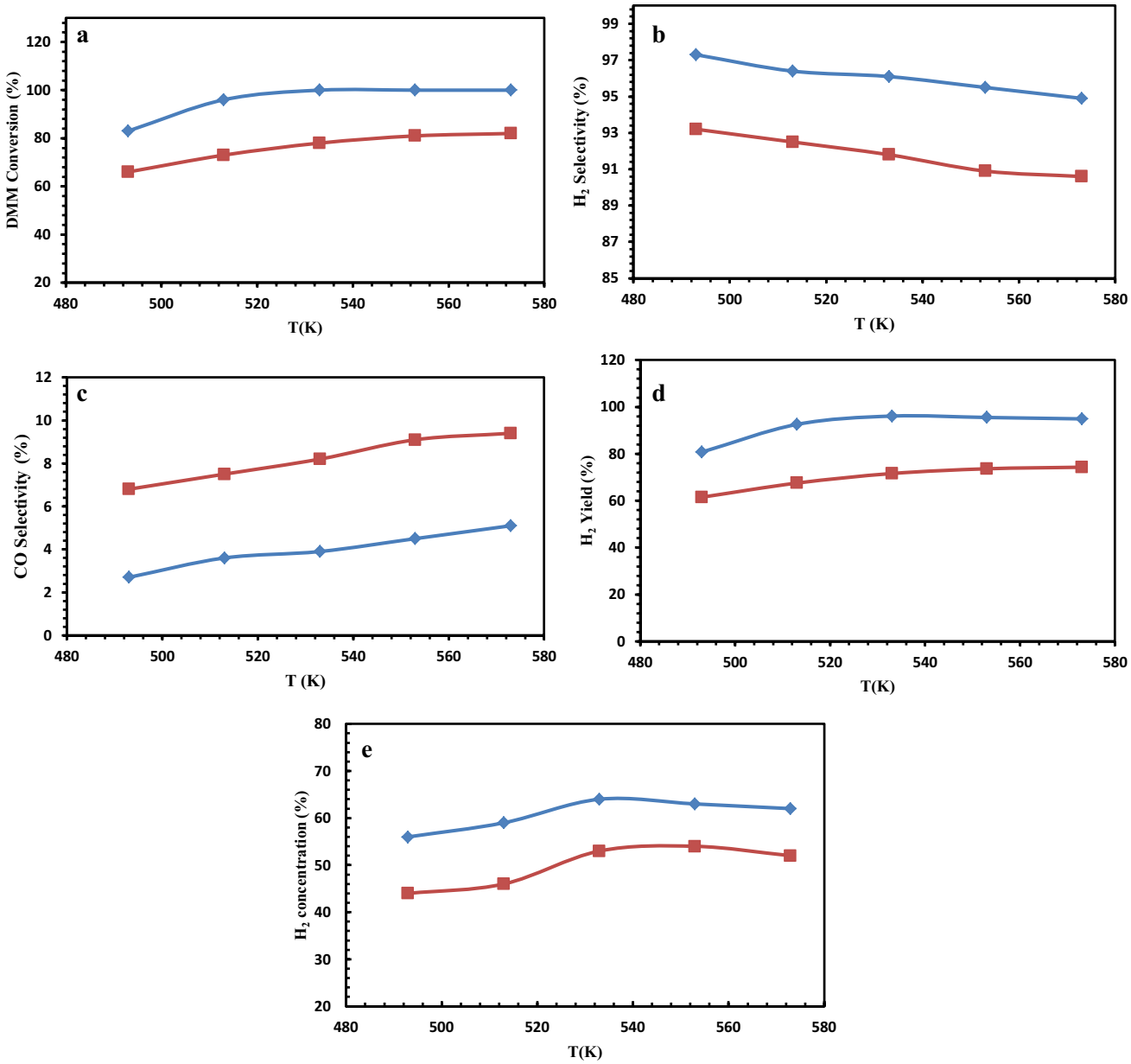

Fig. 8 Influence of reaction temperature on **a** DMM conversion, **b** H_2 selectivity, **c** CO selectivity, **d** H_2 yield and **e** H_2 concentration over $Cu/Zn/Al_2O_3$-AC (blue diamond) and $Cu/Zn/Al_2O_3$ (red square) catalysts. Experimental conditions: GHSV = 20 NL h^{-1} g^{-1}, N_2/H_2O/DMM with 24/5/1 ratio (vol%). (Color figure online)

monitoring of synthesized catalysts was investigated by different methods and was confirmed $Cu/Zn/Al_2O_3$-AC capability for DMM reformation. So that, this catalyst provides 100% DMM conversion with hydrogen productivity of 12.8 L H_2 h^{-1} $g_{cat}{}^{-1}$ and 64% hydrogen concentration at 533 K temperature and GHSV = 20 NL h^{-1} $g_{cat}{}^{-1}$. According to the obtained results and on the fact that DMM is an environmentally friendly compound, we expect it can be a more proper fuel for movable and domestic H_2 sources.

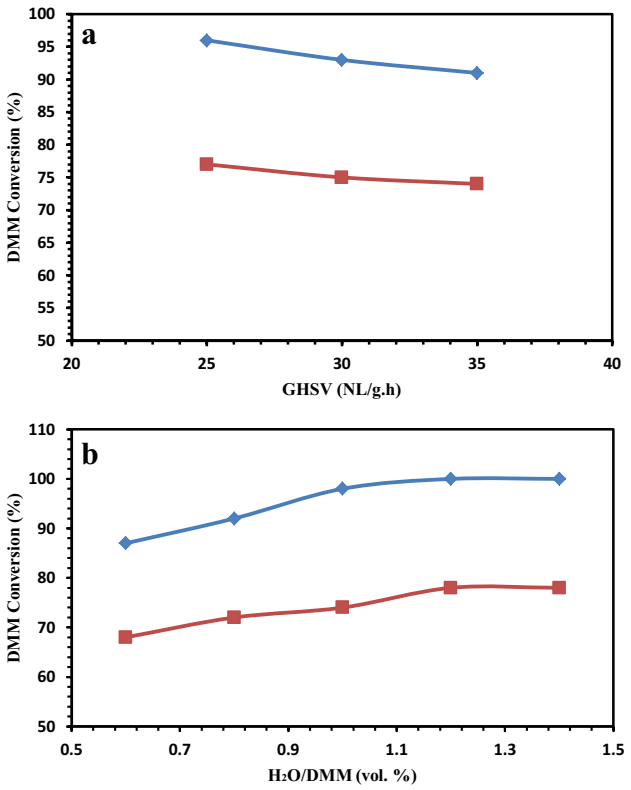

Fig. 9 Influence of **a** GHSV and **b** H_2O to DMM mol ratio on DMM conversion over Cu/Zn/Al_2O_3-AC (blue diamond) and Cu/Zn/Al_2O_3 (red square). Experimental conditions: T = 533 K and GHSV = 20 NL h^{-1} g^{-1} for H_2O to DMM mol ratio on DMM conversion. (Color figure online)

Acknowledgements We acknowledge the support of the Iranian Research Organization for Science and Technology, and Iranian National Science Foundation (INSF).

References

1. K.A. Thavornprasert, M. Capron, L. Jalowiecki-Duhamel, F. Dumeignil, Catal. Sci. Technol. **6**, 958 (2016)
2. D. Franck, M. Capron, B. Katryniok, R. Wojcieszak, A. Löfberg, J.-S. Girardon, S. Desset, M. Araque-Marin, L. Jalowiecki-Duhamel, S. Paul, J. Jpn. Pet. Inst. **58**, 257 (2015)
3. P. Poizot, F. Dolhem, Energ. Environ. Sci. **4**, 2003 (2011)
4. WO Pat. 090294 (2008)
5. EP Pat. 1914293 (2008)
6. R. Chetty, K. Scott, J. Power Sour. **173**, 166 (2007)
7. F. Vigier, C. Coutanceau, J.M. Leger, J.L. Dubois, J. Power Sour. **175**, 82 (2008)
8. K. Thavornprasert, M. Capron, L. Duhamel, O. Gardoll, Appl Catal B Environ. **145**, 126 (2014)
9. J.C. Ball, C. Lapin, J. Buckingham, E. Frame, D. Yost, M. Gonzalez, E. Liney, M. Natarajan, J. Wallace, SAE Trans. Sect. **4**, 2176 (2001)
10. M.M. Maricq, R.E. Chase, D.H. Podsiadlik, W.O. Siegl, E.W. Kaiser, SAE Trans. Sect. **107**, 1504 (1998)
11. Y. Meng, T. Wang, S. Chen, Y. Zhao, X. Ma, J. Gong, Appl. Catal. B: Environ. **160**, 161 (2014)
12. S. Chen, Y. Meng, Y. Zhao, X. Ma, J. Gong, AIChE J. **59**, 2587 (2013)
13. J. Lojewska, J. Wasilewski, K. Terelak, T. Lojewski, A. Kolodziej, Catal. Commun. **9**, 1833 (2008)
14. Y. Fu, J. Shen, Chem. Commun. **21**, 2127 (2007)
15. A. Pechenkin, S. Badmaev, V. Belyaed, V. Sobyanin, Appl. Catal. B Environ. **166**, 166 (2014)
16. T. Kotbagi, D.L. Nguyen, C. Lancelot, C. Lamonier, K.A. Thavornprasert, Z. Wenli, M. Capron, L. Jalowiecki-Duhamel, S. Umbarkar, M. Dongare, F. Dumeignil, Chem. Sus. Chem. **5**, 1467 (2012)
17. T.A. Vu, H.L.G.H. Le, C.D. Dao, L.Q. Dang, K.T. Nguyen, P.T. Dang, H.T.K. Tran, Q.T. Duong, T.V. Nguyen, G.D. Lee, RSC Adv. **78**, 41185 (2014)
18. J.L. Rowsell, O.M. Yaghi, Micropor. Mesopor. Mat. **73**, 3 (2004)
19. F. Maya, C. Palomino Cabello, J.M. Estela, V. Cerdà, G.T. Palomino, Anal. Chem. **87**, 7545 (2015)
20. R. Ricco, L. Malfatti, M. Takahashi, A.J. Hill, P. Falcaro, J. Mater. Chem. A **1**, 13033 (2013)
21. M.Y. Masoomi, S. Beheshti, A. Morsali, J. Mater. Chem. A **2**, 16863 (2014)
22. X. Zhang, X.H. Zang, J.T. Wang, C. Wang, Q.H. Wu, Z. Wang, Microchim. Acta **182**, 2353 (2015)
23. M.Y. Masoomi, M. Bagheri, A. Morsali, Ultrason. Sonochem. **33**, 54 (2016)
24. X. Liu, C. Wang, Z. Wang, Q. Wu, Z. Wang, Microchim. Acta **182**, 1903 (2015)
25. L. Aboutorabi, A. Morsali, Ultrason Sonochem. **28**, 240 (2016)
26. M.Y. Masoomi, A. Morsali, Coordin. Chem. Rev. **256**, 2921 (2012)
27. A. Corma, H. García, F.X. Llabrés i Xamena, Chem. Rev. **110**, 4606 (2010)
28. F. Raoof, M. Taghizadeh, A. Eliassi, F. Yaripour, Fuel **87**, 2967 (2008)
29. W. LiPing, X. Bin, W. Ying, Sci. China Chem. **54**, 1 (2011)
30. S. Lee, S. Park, Int. J. Hydrogen Energy **36**, 8381 (2011)
31. A. Bagheri, M. Taghizadeh, M. Behbahani, A. Asgharinezhad, M. Salarian, A. Dehghani, H. Ebrahimzadeh, M. Amini, Talanta **99**, 132 (2012)
32. T. Semelsberger, K. Ott, R. Borup, H. Greene, Appl. Catal. A **309**, 210 (2006)
33. M. Barrosoa, M. Gomeza, J. Gamboab, L. Arru, J. Phys. Chem. Solids **67**, 1583 (2006)
34. M. Sohrabi, Z. Matbouie, A. Asgharinezhad, A. Dehghani, Microchim Acta **180**, 589 (2013)
35. S.J. Gregg, K.S. Sing, *Adsorption, surface area, and porosity*, (Academic Press, New York, 1982)
36. J. Cai, Y. Fu, Q. Sun, M. Jia, J. Shen, Chin. J. Catal. **34**. 2110 (2013)
37. Z. P. Lu, H. B. Yin, A. L. Wang, J. Hu, W. P. Xue, H. X. Yin, S. X. Liu. J. Ind. Eng. Chem. **37**, 208 (2016)
38. L. Pettersson, K. SjÖStrÖM. Combust. Sci. Tech. **80**, 265 (1991)
39. S. Badmaev, A. Pechenkin, V. Belyaev, V. Sobyanin. Int. J. Hydrogen Energy **1**, 1 (2015)